Zeolites

DOI: 10.1002/anie.201004360

Zeolite Y Crystals with Trimodal Porosity as Ideal Hydrocracking Catalysts**

Krijn P. de Jong, Jovana Zečević, Heiner Friedrich, Petra E. de Jongh, Metin Bulut, Sander van Donk,* Régine Kenmogne, Annie Finiels, Vasile Hulea, and François Fajula**

Zeolites are widely used as microporous acid catalysts in oil refining and petrochemical synthesis.[1] The micropores (ca. 1 nm diameter) provide unique activity and shape selectivity but also induce slow mass transfer of reactants and products.[2] Methods to enhance molecular transport involve synthesis of zeolites with larger micropores (1–2 nm),[3] synthesis of nanosized zeolites (short micropores),[4,5] as well as the creation of mesopores (2–50 nm) in zeolite crystals using acid[6] or base[7,8] leaching, carbon templating,[9] or mesopore structure-directing agents.[10] Results for mesoporous zeolites have been focused largely on MFI type zeolites and have led exclusively to bimodal porosity, that is, micropores and mesopores. It has been argued several times that staged hierarchical porosity should be ideal in catalysis[11] but few examples[12] are known.

One of the most important zeolites applied in catalysis is zeolite Y, which is used in processes such as fluid catalytic cracking, hydrocracking, and alkylation in oil refining and petrochemical synthesis.[6] Advanced methods such as nanosizing and special templating techniques have met limited success for zeolite Y. Generation of mesopores in zeolite Y has been mainly achieved by steaming and acid leaching.[13,14] Limitations of this approach have become apparent based on physisorption and electron tomography studies. Relatively large mesopores (diameter > 20 nm) have been obtained, some of which are in fact cavities that are only connected to the outer surface of the crystals via the micropore network.[13,14] With more-advanced techniques such as templating, small mesopores (2–10 nm) have been realized for zeolite ZSM-5.[10] However, in the latter cases large mesopores were absent and mass transfer limitation in the small mesopores may occur. Based on theoretical considerations it has been proposed that hierarchical pore networks will be optimal for zeolite catalysis.[11,15] Ideally, large mesopores facilitate mass transfer from the surface of the zeolite crystal followed by transport in small mesopores, finally allowing diffusion into short micropores where catalysis takes place. Clearly, no zeolite and in particular zeolite Y with this trimodal porosity is available today. Combinations of acid leaching (dealumination) and base leaching (desilication) hold potential for arriving at trimodal porosity as might be inferred from old[16,17] as well as recent literature.[18]

We have started from a commercially available zeolite H-Y (Zeolyst, CBV 760) that had been previously steamed and acid-leached.[13,14] We refer to this sample as HY-30 in view of its Si/Al atomic ratio (Table 1). Following the systematic studies of Groen et al.,[8] base leaching was carried out with either 0.05 M or 0.10 M aqueous NaOH solutions (Supporting Information, Experimental Section). Base leaching was quenched by acid addition and, subsequently, sodium ions were exchanged for ammonium ions followed by calcination to obtain samples HY-A (0.05 M) and HY-B (0.10 M). Details about the samples summarized in Table 1 comprise the elemental composition (Si/Al ratio), the amount of tetrahedral Al derived from the unit cell size obtained by X-ray diffraction (XRD; expressed by Si/Al_{tet}), and the number of acid sites from temperature-programmed desorption (TPD) of ammonia. Details about the TPD measure-

Table 1: Modification and properties of zeolite Y samples.

Sample	Treatment	Si/Al[a] [at/at]	a_0 [Å]	Si/Al_{tet}[b] [at/at]	Acid sites[c] [mmol g^{-1}]
HY-30	commercial USY zeolite (CBV760)	28.4	24.284	38	0.31
HY-A	HY-30 leached with 0.05 M NaOH	24.8	24.302	27	0.29
HY-B	HY-30 leached with 0.10 M NaOH	20.5	24.311	23	0.30

[a] Si/Al ratio obtained by chemical analysis. [b] Si/Al_{tet} is the atomic ratio of Si over tetrahedrally coordinated Al obtained from unit cell size a_0 determined by XRD analysis ($a_0 \pm 0.007$ Å). [c] Calculated from the amount of NH_3 desorbed (± 0.02 mmol g^{-1}).

[*] K. P. de Jong, J. Zečević, H. Friedrich, P. E. de Jongh
Inorganic Chemistry and Catalysis, Department of Chemistry
Utrecht University
Sorbonnelaan 16, 3584 CA Utrecht (The Netherlands)
E-mail: k.p.dejong@uu.nl
M. Bulut, S. van Donk
Total Research Center Feluy
Zone Industrielle C, 7181 Feluy (Belgium)
E-mail: sander.van-donk@total.com
R. Kenmogne, A. Finiels, V. Hulea, F. Fajula
Institut Charles Gerhardt, UMR 5253 CNRS, UM2, ENSCM, UM1
Ecole Nationale Supérieure de Chimie
8 rue de l'Ecole Normale, 34296 Montpellier Cedex 5 (France)
E-mail: ffajula@enscm.fr

[**] H.F. and K.P.d.J. acknowledge support from the National Research School Combination Catalysis (NRSCC) and from NWO-CW, and P.E.d.J. acknowledges support from NWO-Vidi. Hans Meeldijk is acknowledged for assistance with transmission electron microscopy. The electron tomography studies were carried out in the 3D Electron Microscopy group of Utrecht University headed by Dr. Willie Geerts and Prof. Jan Andries Post. Adri van Laak and Ad Mens were involved in physisorption and Marjan Versluijs in X-ray diffraction measurements.

Supporting information for this article is available on the WWW under http://dx.doi.org/10.1002/anie.201004360.

ments and XRD patterns are given in the Supporting Information (Figures S1 and S2). From these results it appeared that desilication slightly reduced the Si/Al ratio while the amount of zeolitic crystalline phase (estimated from the microporous volume measured by nitrogen adsorption; see below) dropped from 65% for HY-30 to 50% for HY-A to 25% for HY-B. In line with this drop in crystallinity, ^{29}Si NMR (Supporting Information, Figure S3) as well as ^{27}Al NMR spectroscopy (data not shown) indicated a local transformation from crystalline zeolite into amorphous silica–alumina upon treatment with base. Since the crystal shapes were not affected (see below), some of this amorphous material might be present in mesopores.[13] In the remainder of this Communication, we focus on the porosity of the systems since the density (Table 1) and nature (Supporting Information, Figure S2) of the acid sites did not vary largely.

The porosity of the samples was studied by nitrogen physisorption. Figure 1 displays the adsorption–desorption isotherms as well as the pore size distributions (PSDs) derived from the adsorption branches. The data related to these measurements are collected in Table 2. The hysteresis apparent in all isotherms is indicative of mesoporosity. Some mesopore obstruction, suggesting the presence of cavities,[19] is revealed by the closure of the hysteresis loop in the range $p/p_0 = 0.4$–0.5. Many mesopores, however, are open and cylindrical as apparent from the parallel part of the hysteresis loop ($p/p_0 > 0.8$). Upon base leaching, additional mesoporosity is generated as is inferred from both the isotherms and the PSDs in Figure 1. Larger mesopores are enhanced but, much more importantly, small mesopores are boosted and a clear bimodal mesoporosity is observed for the base-leached samples. Since the micropore volume (derived from t-plot analysis) was significant for all samples, we obtained truly trimodal zeolite Y zeolites that contain micropores (ca. 1 nm), small mesopores (ca. 3 nm), and large mesopores (ca. 30 nm). The data in Table 2 reveal that base leaching had more than tripled the volume of small mesopores while the volume of large mesopores only increased by about 50%. Clearly, base leaching is particularly effective in these materials to generate the small-mesopore network. Although the fingerprint of the PSDs in Figure 1 is excitingly clear, we must caution the reader. Physisorption provides average data over many (ca. 10^{12}) zeolite crystals and the data of Figure 1 may originate from truly hierarchical pore networks or from a physical mixture of crystals containing large mesopores and crystals that contain small mesopores. For that reason we carried out a microscopic study to challenge our macroscopic data.

Table 2: Textural properties of zeolite Y samples.

Sample	S_{meso}[a] [$m^2 g^{-1}$]	V_{micro}[b] [$cm^3 g^{-1}$]	V_{meso}[c] [$cm^3 g^{-1}$]	$V_{s\text{-}meso}$[d] [$cm^3 g^{-1}$]	$V_{l\text{-}meso}$[e] [$cm^3 g^{-1}$]	V_{tot}[f] [$cm^3 g^{-1}$]	Pore diameter[g] [nm]	
							small	large
HY-30	213	0.21	0.16	0.07	0.09	0.45	–	28
HY-A	339	0.16	0.25	0.14	0.11	0.51	2.7	27
HY-B	443	0.07	0.37	0.23	0.14	0.55	3.1	27

[a] Mesopore surface area. [b] Micropore volume. [c] Mesopore volume (2–50 nm pores). [d] Volume of small mesopores (2–8 nm pores). [e] Volume of large mesopores (8-50 nm pores). [f] Total pore volume. [g] From PSD (see the Supporting Information, Experimental Section).

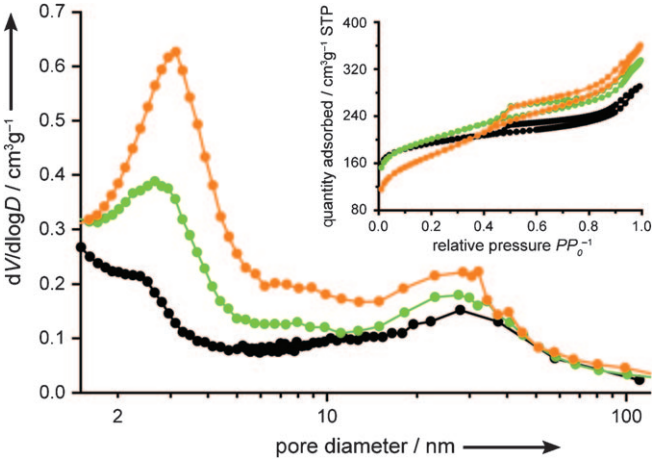

Figure 1. N_2 physisorption analysis of parent HY-30 (black line), base-leached HY-A (green line), and HY-B (orange line) samples. Barrett–Joyner–Halenda (BJH) pore size distributions derived from the adsorption branches of the isotherms (inset) depict the distinct regions of small (ca. 3 nm) and large mesopores (ca. 30 nm). Base leaching predominantly induces the formation of small mesopores. *V*: specific volume; *D*: diameter [nm]; STP: standard temperature and pressure.

Transmission electron microscopy (TEM) is a versatile technique to study nanostructured materials.[20] For imaging mesopores in zeolites, however, TEM does not suffice, and electron tomography (ET)[21–23] based on TEM tilt series was used. 3D reconstructions of zeolite crystals were obtained and analyzed using established methods. Figure 2 presents TEM images as well as numerical cross sections from the tomograms for all three samples. The crystal shape did not change upon leaching, and fragmentation of crystals did not occur on a large scale. From the TEM images (Figure 2a–c), reduced mass density can be inferred for the base-leached samples, but details of the mesopore network could not be derived. The ET results (Figure 2d–f) reveal mesopore details with exceptional clarity. The smooth dark zones in the slices relate to the unaffected microporous regions of the crystal (micropores not imaged), whereas the light gray areas represent the mesopores. For sample HY-30 we observed mainly channel-like mesopores with diameters 15–30 nm well in line with physisorption. Some small cavities with diameters of less than 10 nm are apparent too. Base leaching slightly enhanced the average diameter of the large mesopores, and some surface roughening of the mesopore channels is apparent in Figures 2e and f. Most importantly, a new network of small mesopores with a diameter range of 2–10 nm had been created. These small mesopores were pervasive throughout the crystal and their aspect ratio was well above 1. Analysis of slices of the tomogram (Movies 1–3 in the Supporting Information) revealed that most of the small mesopores

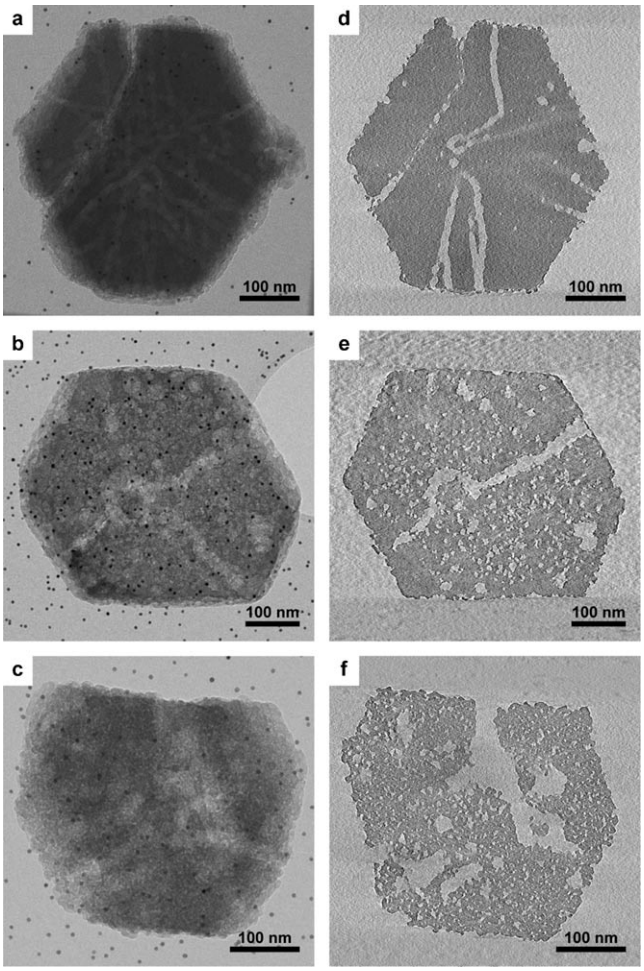

Figure 2. Electron microscopy and electron tomography study of parent HY-30, base-leached HY-A (0.05 M NaOH) and HY-B (0.10 M NaOH) samples. The TEM micrographs show that base leaching of the parent HY-30 (a) leads to generation of more-porous structures as can be seen from HY-A (b) and HY-B (c), yet without revealing the true nature of the mesopore network. The numerical cross-sections through 3D reconstructions of the particles provided by electron tomography clearly depict the presence of both small (ca. 3 nm) and large (ca. 30 nm) mesopores, as well as their interconnectivity and shape: d) 0.56 nm thick slice of HY-30; e) 0.82 nm thick slice of HY-A; f) 0.56 nm thick slice of HY-B sample.

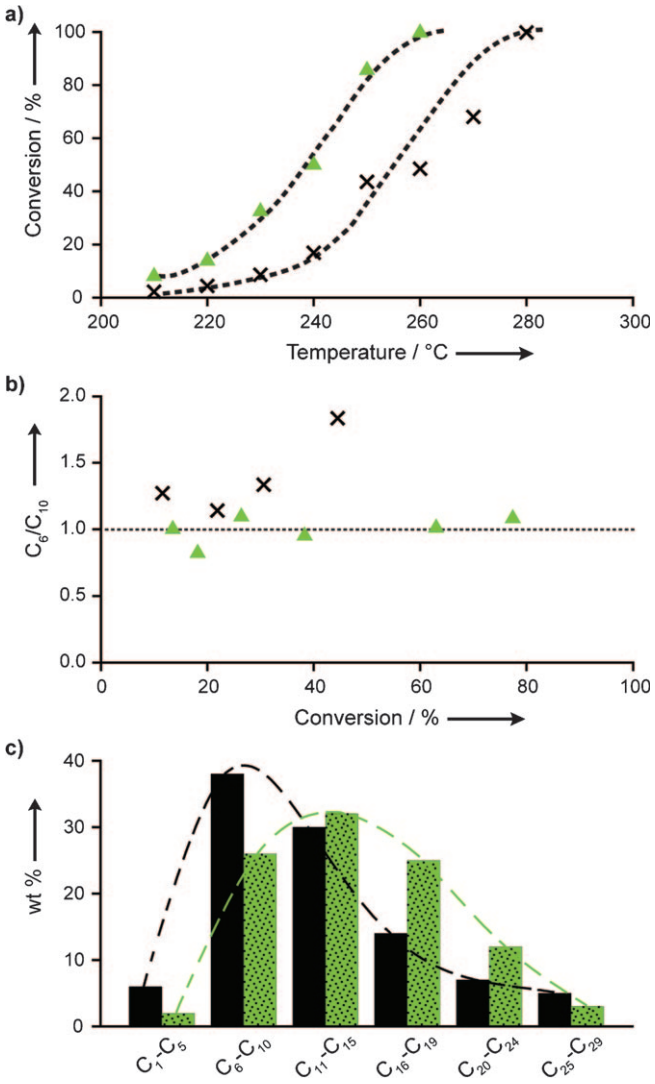

Figure 3. Catalytic testing of parent HY-30 and base-leached HY-A loaded with 0.3 wt% Pt. a) Conversion, b) selectivities in hydrocracking of *n*-hexadecane over Pt/HY-30 (×) and Pt/HY-A (▲). c) Hydrocracking of squalane over Pt/HY-30 (black) and Pt/HY-A (green). For details see text.

were connected either to the large mesopores or to the external surface of the crystals. From detailed studies of several crystals using ET, we concluded that the trimodal porosities of zeolite Y crystals that we obtained are truly hierarchical in nature, that is, micropores, small mesopores, and large mesopores are connected and present in one and the same crystal.

The bifunctional nature of hydrocracking catalysis requires a (de)hydrogenation function.[24] Therefore, hydrocracking catalysis experiments were carried out with H-Y zeolite samples loaded with Pt. Hydrocracking of *n*-hexadecane in the presence of H_2 at 20 bar pressure in a fixed-bed reactor was studied in the temperature range 220–280 °C. The conversions for Pt/HY-30 and Pt/HY-A as a function of temperature are plotted in Figure 3a. The first-order rate constants calculated at 240 °C for the two catalysts were 0.9×10^{-4} and 4.1×10^{-4} g g^{-1} s^{-1}, respectively. To assess the hydrocracking selectivity for *n*-C_{16} alkane, the molar ratio C_6/C_{10} as a function of the conversion is shown in Figure 3b. For Pt/HY-A the ratio was close to unity up to very high conversions, as expected for ideal hydrocracking.[25] For Pt/HY-30 above approximately 30% conversion, the ratio started to increase pointing to secondary cracking of products, thus deviating from ideality. Please note that the *n*-alkane reactant can be considered as a "refractory feedstock" calling for strong acidity of the catalyst. Using squalane (branched C_{30} alkane) at 230 °C, conversion for both catalysts of about 75% was observed, pointing to similar activities for Pt/HY-30 and Pt/HY-A, which might be related to the mild acidity requirements for this reactive feedstock. More importantly, the selectivity patterns for the two catalysts deviated significantly. The product symmetry for Pt/HY-A was preserved, whereas

Pt/HY-30 produced significant amounts of light products (C_1–C_5 alkanes). Clearly, secondary cracking played a role with Pt/HY-30, whereas close to ideal hydrocracking was again observed with Pt/HY-A. For the hydrocracking of vacuum gas oil (VGO), a $NiMoS_2$/zeolite Y/alumina extruded catalyst was prepared, incorporating HY-A as zeolite Y phase. The catalyst was evaluated and compared with a state-of-the art commercial catalyst under industrially relevant conditions in the temperature range 360–390 °C and at a pressure of 155 bar for around 200 h. The results are summarized in Table 3 and reveal that for the HY-A based catalyst the yield towards middle distillates (diesel and kerosene), compared at equal conversions of 80%, was dramatically enhanced along with a significant decrease of the less desired naphtha. Moreover, coke formation over the HY-A based catalyst was significantly reduced, indicating higher catalyst stability as a direct benefit from its enhanced porosity. The activity of HY-A was lower than that of the commercial catalyst as the temperature required for 80% conversion had increased by 13 °C.

Table 3: Comparison of hydrocracking of VGO over $NiMoS_2$/HY-A/alumina and over a commercial catalyst.[a]

activity[b] ΔT [°C]		+13
selectivity[c] [Δwt%]	lights (<65 °C)	−4.3
	naphtha (65–145 °C)	−5.6
	kerosene (145–250 °C)	+5.2
	diesel (250–375 °C)	+4.7
coke formation[d] [Δwt%]		−22

[a] All data are relative to the commercial catalyst. Reaction conditions: 155 bar; H_2/feed ratio: 800 NL/L; liquid hourly space velocity (LHSV): 2.43 h^{-1}. Pretreated VGO feed: 8 ppm N, 15 ppm S and 0.8707 g mL^{-1} density at 15 °C. [b] Temperatures required to reach 80% conversion. [c] Values reported at 80% conversion of VGO after ca. 200 h on stream. [d] Coke yield after ca. 200 h on stream.

With zeolite Y, an intracrystalline trimodal porosity involving micropores (from the zeolite synthesis), smaller sponge-like mesopores (from desilication), and large mesopores (from steaming and acid leaching) was obtained. The hierarchical trimodal nature of the pore system is proposed to be beneficial for rapid mass transfer of hydrocracking products from the micropores, thus almost fully suppressing secondary cracking. This conclusion is qualitatively in line with the recently introduced hierarchy factor.[26] With respect to the mechanism of the generation of the small mesopores (2–10 nm), we speculate that the structure of zeolite Y may play an important role. By removing the tetrahedrally coordinated atoms between supercages, we expect a mesopore of about 3 nm in width. Acid leaching might generate nuclei for these mesopores by starting to break down the walls between supercages in line with small cavities (ca. 2 nm) observed (Figure 2d). Growth and in particular elongation (aspect ratio > 1) of these nuclei for mesopores is proposed to be brought about by desilication (Figure 2e,f). Future work will involve studies of other zeolites (such as mordenite), molecular modeling of the framework changes, as well as full image analysis of the mesopore network in zeolites. Trimodal hierarchical porosity in zeolites and related materials (e.g., MOF,[27] COF[28]) can play an important role in catalysis, as demonstrated by the current work, as well as in adsorption, diffusion, and separation applications.

Experimental Section

The starting material to which we refer as HY-30 is commercially available steamed and acid-leached zeolite H-Y purchased from Zeolyst under sample code CBV760. The parent HY-30 sample was submitted to desilication treatment with 0.05 M or 0.10 M NaOH solution at room temperature for 15 min, which led to the formation of highly mesoporous samples HY-A and HY-B, respectively. Electron tomography of the obtained mesoporous zeolites was performed on a Tecnai 20 transmission electron microscope operated at 200 kV. Images of the particles were collected over a tilt range of ±75° with 1° or 2° tilt increments at nominal magnifications of 19 k or 29 k. Alignment of the TEM tilt series and 3D reconstructions of the investigated particles were performed using IMOD software.[29] The resolution in the reconstructions was sufficient to visualize mesopores down to 2 nm in diameter. Catalytic performances of the Pt-loaded (0.3 wt% Pt) parent and desilicated zeolite samples were measured for hydrocracking of *n*-hexadecane or squalane. Zeolite HY-A was extruded with alumina binder and loaded with nickel and molybdenum to arrive at NiMo/HY-A/Al_2O_3 catalysts for hydrocracking of vacuum gas oil.

Received: July 16, 2010

Keywords: cracking · electron microscopy · mesoporous materials · microporous materials · zeolites

[1] A. Corma, *Chem. Rev.* **1995**, *95*, 559–614.
[2] D. M. Ruthven, M. F. M. Post, *Stud. Surf. Sci. Catal.* **2001**, *137*, 525–577.
[3] A. Corma, M. J. Díaz-Cabãas, J. L. Jordá, C. Martínez, M. Moliner, *Nature* **2006**, *443*, 842–845.
[4] G.-T. Vuong, T.-O. Do, *J. Am. Chem. Soc.* **2007**, *129*, 3810–3811.
[5] M. Choi, K. Na, J. Kim, Y. Sakamoto, O. Terasaki, R. Ryoo, *Nature* **2009**, *461*, 246–250.
[6] S. van Donk, A. H. Janssen, J. H. Bitter, K. P. de Jong, *Catal. Rev. Sci. Eng.* **2003**, *45*, 297–319.
[7] J. C. Groen, W. Zhu, S. Brouwer, S. J. Huynink, F. Kapteijn, J. A. Moulijn, J. Pérez-Ramirez, *J. Am. Chem. Soc.* **2007**, *129*, 355–360.
[8] J. C. Groen, J. A. Moulijn, J. Pérez-Ramírez, *J. Mater. Chem.* **2006**, *16*, 2121–2131.
[9] K. Egeblad, C. H. Christensen, M. Kustova, C. H. Christensen, *Chem. Mater.* **2008**, *20*, 946–960.
[10] D. H. Park, S. S. Kim, H. Wang, T. J. Pinnavaia, M. C. Papapetrou, A. A. Lappas, K. S. Triantafyllidis, *Angew. Chem.* **2009**, *121*, 7781–7784; *Angew. Chem. Int. Ed.* **2009**, *48*, 7645–7648.
[11] G. Wang, E. Johannessen, C. R. Kleijn, S. W. de Leeuw, M.-O. Coppens, *Chem. Eng. Sci.* **2007**, *62*, 5110–5116.
[12] W. Schmidt, *ChemCatChem* **2009**, *1*, 53–67.

[13] A. H. Janssen, A. J. Koster, K. P. de Jong, *Angew. Chem.* **2001**, *113*, 1136 – 1138; *Angew. Chem. Int. Ed.* **2001**, *40*, 1102 – 1104.
[14] A. H. Janssen, A. J. Koster, K. P. de Jong, *J. Phys. Chem. B* **2002**, *106*, 11905 – 11909.
[15] M. Hartmann, *Angew. Chem.* **2004**, *116*, 6004 – 6006; *Angew. Chem. Int. Ed.* **2004**, *43*, 5880 – 5882.
[16] R. L. V. Mao, S. Xiao, A. Ramsaran, J. Yao, *J. Mater. Chem.* **1994**, *4*, 605 – 610.
[17] R. L. V. Mao, A. Ramsaran, S. Xiao, J. Yao, V. Semmer, *J. Mater. Chem.* **1995**, *5*, 533 – 535.
[18] X. Li, R. Prins, J. A. van Bokhoven, *J. Catal.* **2009**, *262*, 257 – 265.
[19] P. I. Ravikovitch, A. V. Neimark, *Langmuir* **2002**, *18*, 9830 – 9837.
[20] M. W. Anderson, T. Ohsuna, Y. Sakamoto, Z. Liu, A. Carlsson, O. Terasaki, *Chem. Commun.* **2004**, 907 – 916.
[21] P. A. Midgley, E. P. W. Ward, A. B. Hungría, J. M. Thomas, *Chem. Soc. Rev.* **2007**, *36*, 1477 – 1494.
[22] O. Ersen, C. Hirlimann, M. Drillon, J. Werckmann, F. Tihay, C. Pham-Huu, C. Crucifix, P. Schultz, *Solid State Sci.* **2007**, *9*, 1088 – 1098.
[23] H. Friedrich, P. E. de Jongh, A. J. Verkleij, K. P. de Jong, *Chem. Rev.* **2009**, *109*, 1613 – 1629.
[24] F. Alvarez, F. R. Ribeiro, G. Perot, C. Thomazeau, M. Guisnet, *J. Catal.* **1996**, *162*, 179 – 189.
[25] J. W. Thybaut, C. S. L. Narashiman, J. F. Denayer, G. V. Baron, P. A. Jacobs, J. A. Martens, G. B. Marin, *Ind. Eng. Chem. Res.* **2005**, *44*, 5159 – 5169.
[26] J. Peìrez-Ramiìrez, S. Abelloì, A. Bonilla, J. C. Groen, *Adv. Funct. Mater.* **2009**, *19*, 164 – 172.
[27] M. Eddaoudi, J. Kim, N. Rosi, D. Vodak, J. Wachter, M. O'Keeffe, O. M. Yaghi, *Science* **2002**, *295*, 469 – 472.
[28] A. P. Côte, A. I. Benin, N. W. Ockwig, M. O'Keeffe, A. J. Matzger, O. M. Yaghi, *Science* **2005**, *310*, 1166 – 1170.
[29] J. R. Kremer, D. N. Mastronarde, J. R. McIntosh, *J. Struct. Biol.* **1996**, *116*, 71 – 76.

